



## Ship-based measurement of air-sea CO<sub>2</sub> exchange by eddy covariance

Scott D. Miller,<sup>1</sup> Christa Marandino,<sup>2,3</sup> and Eric S. Saltzman<sup>2</sup>

Received 6 April 2009; revised 15 July 2009; accepted 1 September 2009; published 22 January 2010.

[1] A system for the shipboard measurement of air-sea CO<sub>2</sub> fluxes by eddy covariance was developed and tested. The system was designed to reduce two major sources of experimental uncertainty previously reported. First, the correction for in situ water vapor fluctuations (the “Webb” correction) was reduced by 97% by drying the air sample stream. Second, motion sensitivity of the gas analyzer was reduced by using an open-path type sensor that was converted to a closed-path configuration to facilitate drying of the air stream. High-quality CO<sub>2</sub> fluxes were obtained during 429 14 min flux intervals during two cruises in the North Atlantic. The results suggest that the gas analyzer resolved atmospheric CO<sub>2</sub> fluctuations well below its RMS noise level. This noise was uncorrelated with the vertical wind and therefore filtered out by the flux calculation. Using climatological data, we estimate that the techniques reported here could enable high-quality measurements of air-sea CO<sub>2</sub> flux over much of the world oceans.

**Citation:** Miller, S. D., C. Marandino, and E. S. Saltzman (2010), Ship-based measurement of air-sea CO<sub>2</sub> exchange by eddy covariance, *J. Geophys. Res.*, 115, D02304, doi:10.1029/2009JD012193.

### 1. Introduction

[2] The exchange of carbon dioxide across the air-sea interface is an important component of the atmospheric CO<sub>2</sub> budget. Understanding how future changes in climate will affect oceanic uptake and release of CO<sub>2</sub> requires a process-oriented understanding of the factors controlling the air-sea CO<sub>2</sub> flux,  $F_c$ . The flux is typically expressed as

$$F_c = k(C_w - C_a/\alpha), \quad (1)$$

where  $C_w$  and  $C_a$  are the bulk seawater and air concentrations,  $\alpha$  is the dimensionless solubility, and  $k$  is the piston velocity or gas transfer coefficient. The piston velocity in equation (1) is typically parameterized on the basis of geochemical tracers such as dual tracer experiments or <sup>14</sup>C [Nightingale *et al.*, 2000; Wanninkhof, 1992]. Flux measurements using the micrometeorological technique eddy covariance (EC) have also been used to provide a direct measurement of the piston velocity. EC resolves fluxes at spatial (1–10 km) and temporal (1 h) scales well matched to the atmospheric and oceanic forcing of gas exchange. However, few EC-based air-sea CO<sub>2</sub> flux studies have been published due to the difficulty in making these measurements from ships at sea [McGillis *et al.*, 2001, 2004; Kondo and Tsukamoto, 2007]. Improvements in the methodology for air-sea CO<sub>2</sub> flux measurements are necessary to reduce uncertainties in air-sea fluxes and to expand the global flux database.

[3] The EC approach involves the measurement of the turbulent CO<sub>2</sub> flux as  $F_c = \overline{\rho_a w'c'}$ , where  $\rho_a$  is the dry air density,  $w$  is the vertical component of wind velocity, and  $c$  is the dry air mixing ratio of CO<sub>2</sub>. The primes denote fluctuations about the mean value, sampled fast enough (typically 10 Hz) to capture the smallest flux-carrying atmospheric eddies, and the averaging interval for the covariance is long enough (typically 15–60 min) to include the large-scale atmospheric eddies contributing to the turbulent flux [Kaimal and Finnigan, 1994]. Early EC measurements of air-sea CO<sub>2</sub> flux in coastal environments yielded fluxes that were unrealistically high relative to estimates based on the global <sup>14</sup>C budget or deliberate tracer experiments [Smith and Jones, 1985, 1986; Broecker *et al.*, 1986]. Subsequently, McGillis *et al.* [2001] reported ship-based EC CO<sub>2</sub> fluxes in general agreement with tracer techniques. Their methodology overcame many of the challenges in making EC measurements at sea, including motion effects on the wind vector [Edson *et al.*, 1998]. McGillis *et al.* [2001] also quantified two major sources of uncertainty in the measurement of CO<sub>2</sub> fluxes over the ocean. In situ water vapor fluctuations (the “Webb” correction [Webb *et al.*, 1980]) required a correction that averaged 45% of the true CO<sub>2</sub> flux, and motion sensitivity of the CO<sub>2</sub> signal from a commercially available closed-path InfraRed Gas Analyzer (IRGA, LI6262, LiCor Inc.) required a correction that averaged 30% of the true CO<sub>2</sub> flux.

[4] This paper describes the design and operational characteristics of a system for shipboard measurements of air-sea CO<sub>2</sub> flux by eddy covariance. An effort was made to minimize the two major sources of uncertainty identified by McGillis *et al.* [2001]. CO<sub>2</sub> flux data from two cruises in the North Atlantic are presented to demonstrate system performance under field conditions. We then combine our results with climatological data to estimate the fraction of the global ocean that is amenable to direct air-sea CO<sub>2</sub> flux

<sup>1</sup>Atmospheric Sciences Research Center, State University of New York at Albany, Albany, New York, USA.

<sup>2</sup>Earth System Science, University of California, Irvine, California, USA.

<sup>3</sup>Now at Leibniz Institut für Meereswissenschaften, Kiel, Germany.



**Figure 1.** R/V *Knorr*. Anemometers, the motion sensor, GPS, and gas inlets were mounted to the bow mast (inset), approximately 14 m above the ocean surface. Gas analyzers were located in the bosun's locker, directly below the mast.

measurements using these techniques. Comparison of piston velocities for CO<sub>2</sub> and dimethylsulfide measured in situ during these cruises were reported in a previous paper [Miller *et al.*, 2009].

## 2. Methods

[5] The measurements were made during two cruises on the research vessel R/V *Knorr* in the summer of 2007. The

first cruise (Knorr-07a) was from Bridgetown, Barbados (13°06'N, 59°37'W) to Reykjavik, Iceland (64°10'N, 21°57'W) and lasted 14 days (29 May to 9 June). The second cruise (Knorr-07b) was from Reykjavik to Woods Hole, MA (41.52°N, -70.66°W) and lasted 10 days (17–26 July).

### 2.1. Wind Vector

[6] Sensors were mounted at the foremost location on the *Knorr*'s 8 m tall bow mast (Figures 1 and 2). The wind vector was measured using two 3-axis ultrasonic (sonic) anemometers (CSAT3, Campbell Scientific, Logan, UT) approximately 6 m above *Knorr*'s main deck and 14 m above the mean ocean surface. The two sonic anemometers were located 2 m forward of the bow mast, and separated horizontally by 1 m, one sensor portside of the mast and the other starboard. An inertial motion sensor (MotionPak 2, Systron Donner, Walnut Creek, CA) measured linear accelerations and angular rates along 3 orthogonal axes. The motion sensor was located between and slightly aft of the sonic anemometers, 0.75 m from their measurement volumes, and the orientation of anemometers relative to the motion sensor was fixed. A GPS receiver (GPS 16, Garmin International, Olathe, KS) provided ship speed and heading.

### 2.2. Atmospheric CO<sub>2</sub> and H<sub>2</sub>O

[7] Commercially available IRGAs include “open-path” and “closed-path” configurations. The open-path style sensor has its measurement volume exposed to the atmosphere, and is mounted next to the sonic anemometer. Closed-path sensors are located separately from the sonic

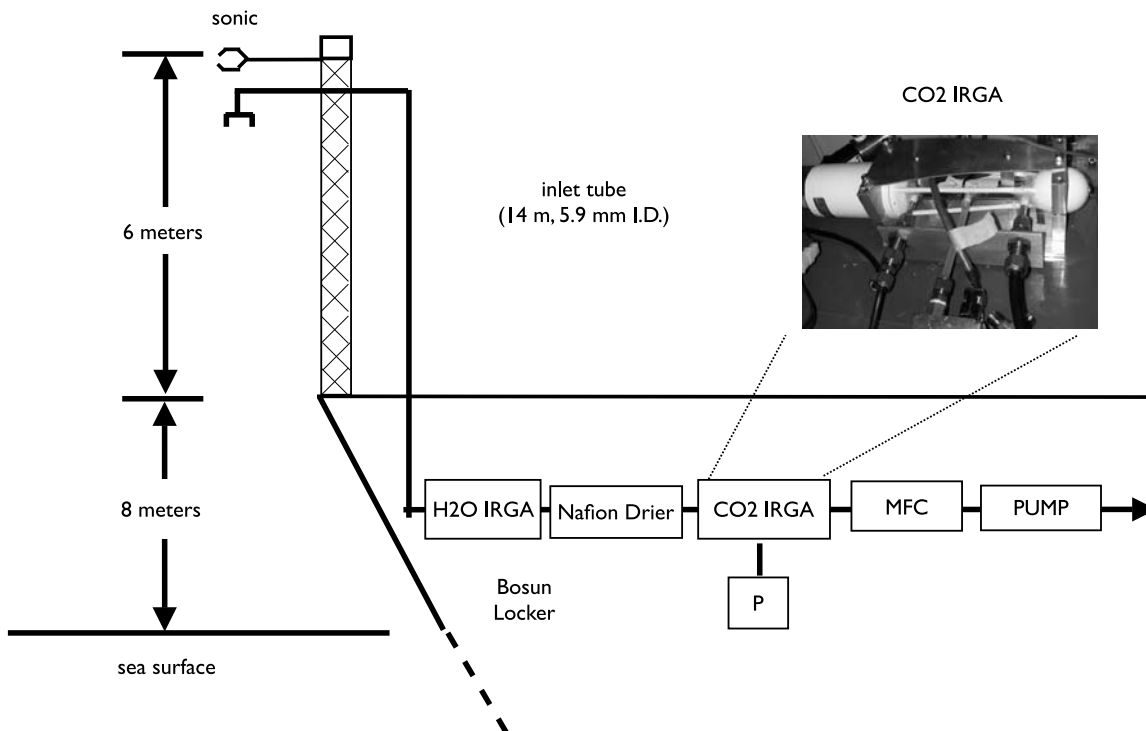


**Figure 2.** Bosun locker layout of the system to measure CO<sub>2</sub> flux, where “MFC” is mass flow controller and “P” is pressure sensor. The CO<sub>2</sub> IRGA was an open-path-style sensor (LI7500, LiCor, Inc.) that was converted to a closed-path sensor. A custom-made aluminum cradle was used for rigidity (inset photo).

anemometer and sample air is drawn by a pump from an air inlet collocated with the sonic anemometer. The flow of the air sample through the tubing results in a time delay between its entrance to the inlet and its sampling by the IRGA, and also to degradation of the turbulent fluctuations due to interactions between the air stream and the walls of the tubing. Many studies have examined these effects [e.g., *Leuning and Judd*, 1996]. Over the ocean, the main advantage of open-path systems, the absence of tubing-related signal degradation, is overshadowed by the necessity of large corrections for the effects of sensible and latent heat flux (or “Webb” corrections, discussed in detail in section 2.4.1). The Webb correction for water vapor (i.e., latent heat) flux was found by *McGillis et al.* [2001] to be 45% of the true CO<sub>2</sub> flux during their study. More practically, the performance of open-path sensors exposed to the marine atmosphere can degrade quickly (over a period of hours) due to the accumulation of salt spray on the sensor windows.

[8] Closed-path sensors can be configured to minimize the effects of the Webb corrections (discussed in detail in section 2.4.1), and methods exist to correct for signal degradation due to flow through the sample tube [*Leuning and Moncrieff*, 1990; *Massman*, 2000]. However, the CO<sub>2</sub> signal returned by closed-path sensors has been found to be sensitive to platform motion. *McGillis et al.* [2001] found that this contamination resulted in a CO<sub>2</sub> flux bias that was 30% of the true CO<sub>2</sub> flux. The approach used in this study was to combine the advantages of the two sensor styles by converting an open-path sensor (less sensitive to motion errors) to a closed-path configuration (reducing the Webb corrections and data loss due to fouling of sensor windows by sea spray).

[9] Air sampled at the bow mast inlet was analyzed using two fast-response IRGAs plumbed in series (Figure 2) and located in the bosun locker directly below the bow mast (Figures 1 and 2). The “H<sub>2</sub>O IRGA” (LI7000, LiCor Inc.) was used to calculate the water vapor flux, and the “CO<sub>2</sub> IRGA” (LI7500, LiCor, Inc.) was used to calculate the CO<sub>2</sub> flux. The H<sub>2</sub>O IRGA was a closed-path style sensor, while the CO<sub>2</sub> IRGA was an open-path style sensor that was converted to a closed-path configuration by inserting a cylindrical glass cell (12.5 cm long, 1.6 cm internal diameter (I.D.), volume 0.025 L) into the optical path. The instrument “head” was rigidly supported by a custom-made aluminum mount (Figure 2). Air was drawn to the IRGAs at 16–18 slpm from a filtered inlet (90 mm diameter, 1 micron) centered between the sonic anemometers. The air was drawn through 14m of 5.9 mm I.D. polyethylene-lined Dekabon 1300 tubing (Saint Gobain, Garden Grove, CA). The travel time of air in the tubing was approximately 1.2 s, determined empirically both by adding a standard gas step response CO<sub>2</sub> concentration change at the inlet and by finding the maximum correlation between sonic anemometer temperature and CO<sub>2</sub> concentration in the IRGA cell. The flushing time for the measurement volume of each of the sensors was less than 0.1 s.

### 2.3. Calculation of Turbulent Fluxes

[10] Turbulent air-sea fluxes of momentum, heat, and CO<sub>2</sub> were calculated according to

Momentum

$$\tau_x = -\overline{\rho_a u'w'}, \quad (2)$$

Sensible heat

$$H = \overline{\rho_a c_p w'T'}, \quad (3)$$

Latent heat

$$H_L = \overline{\rho_a L_v w'q'}, \quad (4)$$

Carbon dioxide

$$F_c = \overline{\rho_a w'c'}, \quad (5)$$

where  $\tau_x$  is the momentum flux in the along-wind ( $x$ ) direction,  $u$  is the along-wind component of wind velocity,  $H$  is sensible heat flux,  $H_L$  is latent heat flux,  $c_p$  is specific heat capacity of air,  $T$  is dry air temperature,  $L_v$  is latent heat of vaporization, and  $q$  is specific humidity.

## 2.4. CO<sub>2</sub> Flux Corrections

### 2.4.1. Density Correction

[11] The CO<sub>2</sub> flux is defined in terms of CO<sub>2</sub> mixing ratio  $c$  (equation (5)). The IRGAs do not measure CO<sub>2</sub> mixing ratio, rather they measure the CO<sub>2</sub> molar density ( $\rho_c$ ) between the source and detector. In addition to changes in the CO<sub>2</sub> mixing ratio, changes in air density due to water vapor, temperature, and pressure will affect the measured molar density. To extract the CO<sub>2</sub> fluctuations and flux, this “contamination” requires a correction (the Webb correction) to remove the portion of the measured CO<sub>2</sub> molar density caused by the background air density fluctuations. The correction is given by

$$F_c = \overline{w'\rho'_c} + (1 + \mu\sigma) \frac{\overline{\rho'_c}}{\overline{T}} \overline{w'T'} + \mu \frac{\overline{\rho'_c}}{\overline{\rho_a}} \overline{w'\rho'_v} + (1 + \mu\sigma) \frac{\overline{\rho'_c}}{\overline{P}} \overline{w'P'}, \quad (6)$$

where  $\rho_v$  is the molar density of H<sub>2</sub>O,  $\sigma = \rho_v/\rho_a$ ,  $\mu = M_a/M_v$ ,  $M$  is molecular weight, subscripts “a” and “v” refer to dry air and water vapor, respectively, and  $P$  is pressure [*Webb et al.*, 1980]. The first term on the right hand side (rhs) of equation (6) is the uncorrected CO<sub>2</sub> flux, and the second, third, and fourth terms are the Webb corrections for temperature, water vapor, and pressure fluctuations in the IRGA cell, respectively. For closed-path systems, temperature fluctuations are eliminated by heat exchange as the air sample travels through the inlet tubing, and therefore the second term on rhs of equation (6) is negligible. This was confirmed by laboratory tests using the same tubing and flow configuration as the Knorr-07 cruises (data not shown). Air density fluctuations due to turbulent pressure fluctuations are also routinely assumed to be negligible [*Webb et al.*, 1980]; however, they are retained here to account for

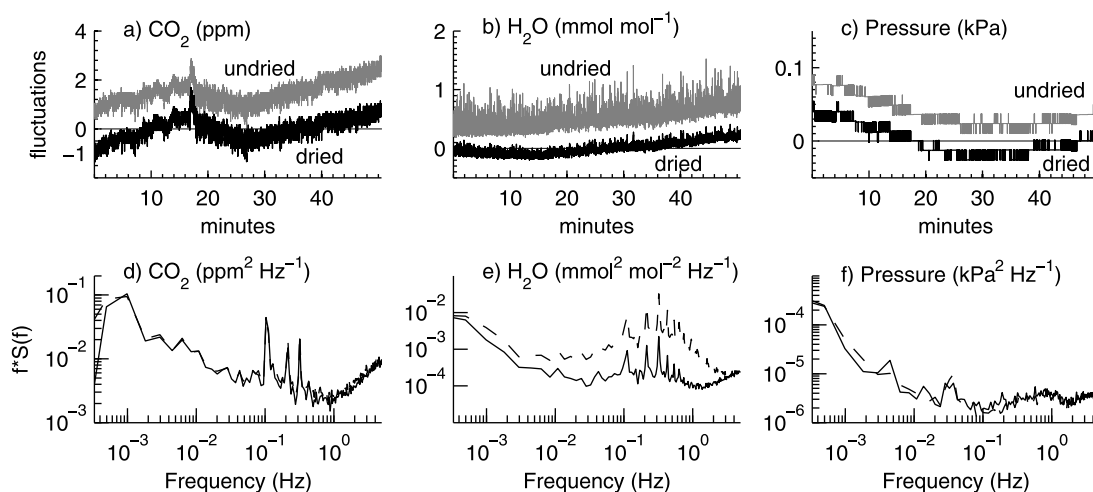


**Figure 3.** Laboratory tests on Nafion drier effects on (a and d) CO<sub>2</sub> (ppm), (b and e) H<sub>2</sub>O (mmol mol<sup>-1</sup>), and (c and f) pressure (kPa) fluctuations. Figures 3a–3c show 50 minute time series with mean removed for the “dried” (dark curve) and “undried” (light curve) signals, with the undried curve offset vertically for clarity. Figures 3d–3f show power spectra of air sampled upstream (undried; dashed curve) and downstream (dried; solid curve) of the Nafion drier.

hydrostatic pressure fluctuations due to ship heave (discussed in section 2.4.2).

[12] The Webb correction for water vapor (i.e., latent heat) flux was found by *McGillis et al.* [2001] to be 45% of the true CO<sub>2</sub> flux. In this study, the CO<sub>2</sub> flux contamination due to water vapor fluctuations was treated differently than *McGillis et al.* [2001] in two ways. First, instead of measuring the water vapor flux and making a large correction to the CO<sub>2</sub> flux according to equation (6), a Nafion multitube membrane drier (PD-200T, PermaPure) with a dry air counter flow was used to remove water vapor fluctuations in the CO<sub>2</sub> IRGA cell (Figure 2). The reduction of the water vapor flux reduced the associated Webb correction, the third term on the rhs of equation (6). The performance of the Nafion tubing was tested in the laboratory, as shown by the time series and spectra of CO<sub>2</sub>, H<sub>2</sub>O, and pressure fluctuations in Figure 3. The Nafion had negligible impact on CO<sub>2</sub> (Figures 3a and 3d) and pressure (Figures 3c and 3f) fluctuations while dramatically reducing the water vapor fluctuations (Figures 3b and 3e). The elimination of water vapor fluctuations markedly reduced the Webb correction (see section 3). The combination of the Nafion with the elimination of temperature fluctuations in the tubing therefore provides significant advantages relative to open-path sensors or closed-path sensors with an undried air stream.

[13] The second difference in our approach was to apply the Webb correction for residual water vapor and temperature fluctuations on a sample-by-sample (10 Hz) basis, rather than use the averaged fluxes according to equation (6). The advantage of the sample-by-sample correction is that a time series of the CO<sub>2</sub> mixing ratio is obtained, which can be used to calculate turbulence statistics and spectra. Because of the Webb contamination, statistics and spectra based on CO<sub>2</sub> density (not mixing ratio) are coupled with water vapor and temperature statistics and spectra [*Iwata et al.*, 2005].

The sample-by-sample Webb correction was calculated by applying the Ideal Gas Law according to

$$c = (\rho_c / \rho_a) M_a / M_c, \quad (7)$$

$$\rho_a = P_a / RT, \quad (8)$$

$$P_a = P - P_v, \quad (9)$$

$$P_v = \rho_v RT, \quad (10)$$

where the density of CO<sub>2</sub> and H<sub>2</sub>O molecules ( $\rho_c$  and  $\rho_v$ ) between the source and detector were measured by the IRGA,  $R$  is the gas constant, and  $P_a$  and  $P_v$  are the partial pressures of dry air and water vapor. Field data have shown the corrected CO<sub>2</sub> fluxes using the conventional method (equation (6)) and the sample-by-sample approach (equations (7)–(10)) to be equivalent [*Miller et al.*, 2004].

#### 2.4.2. Ship Heave Effects on CO<sub>2</sub> Measurement

[14] Air density fluctuations due to turbulent pressure fluctuations in the IRGA cell are routinely assumed negligible; however, nonturbulent pressure fluctuations can be important on a moving ship. Ship heave motions can induce vertical displacements of order 10 m during high seas, giving rise to pressure fluctuations on the order of 1 mbar. For a background CO<sub>2</sub> mixing ratio of 380 ppm, this corresponds to an apparent CO<sub>2</sub> fluctuation of 0.4 ppm, which is similar to or larger than the true atmospheric fluctuations in CO<sub>2</sub>. In this study, pressure in the CO<sub>2</sub> IRGA cell was measured with a high resolution (0.03 mbar), fast-response (50 Hz) pressure sensor capable of resolving the hydrostatic fluctuations due to ship heave (Model 6110,

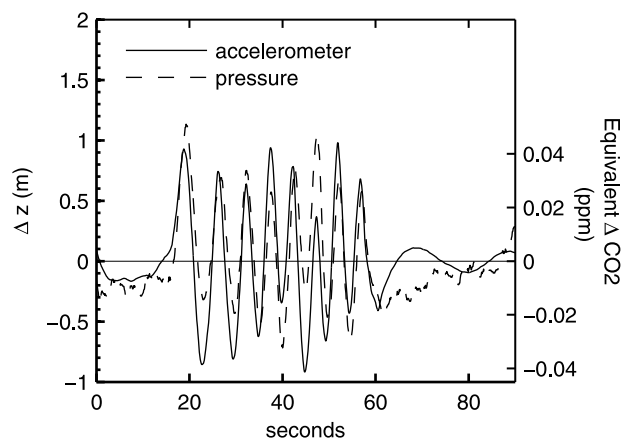


**Figure 4.** Laboratory tests showing heave-induced apparent CO<sub>2</sub> fluctuations. Time series of vertical displacement (meters, left axis) calculated by integrating twice the vertical acceleration (solid curve) and calculated from the fast response pressure measurement and the hydrostatic equation. The right axis shows equivalent CO<sub>2</sub> fluctuations (ppm) calculated from the pressure fluctuations assuming background CO<sub>2</sub> concentration of 380 ppm.

Mensor Corp., San Marcos, TX, Figure 2). The measured pressure was used in the calculation of the dry air density (equation (9)). Thus, the pressure correction for ship heave was applied analogous to the Webb correction for water vapor fluctuations in the sample cell. To our knowledge, the effect of heave-induced pressure fluctuations on ship-based eddy covariance air-sea CO<sub>2</sub> flux has not been considered previously.

[15] If the heave-induced fluctuations are completely uncorrelated with the vertical wind, they will not contribute to the flux. However, there are several reasons why the vertical wind may contain spurious components that have nonzero correlation with the heave, including incomplete or imperfect motion correction of the wind vector, a residual vertical wind contamination due to flow distortion about the ship, mounting hardware, or nearby sensors, and correlations between ship motion and flow distortion that result in residual motion-induced components in the vertical wind vector. “Real” wave-induced correlations between pressure and vertical wind may also exist in the near surface layer [Hristov *et al.*, 2003], though these are likely much smaller than the hydrostatic fluctuations.

[16] The effect of heave-induced hydrostatic pressure fluctuations was demonstrated in laboratory tests using a pulley to raise and lower a package consisting of a pressure sensor and the Motion Pak II by about 2 m (Figure 4). The vertical displacement of the package was calculated both by integrating the vertical acceleration and by using the measured pressure sensor and the hydrostatic equation, with good agreement (Figure 4., left axis). The equivalent CO<sub>2</sub> fluctuations were calculated based on the heave-induced pressure fluctuations (Figure 4, right axis). Figure 4 shows that even small vertical displacements can induce apparent CO<sub>2</sub> fluctuations that are of similar order to real atmospheric CO<sub>2</sub> fluctuations over the ocean.

### 2.4.3. IRGA Motion-Induced Errors

[17] In addition to the effect of pressure on air density, the accelerations caused by ship motion result in spurious CO<sub>2</sub> signals in closed-path IRGAs (LI6262 and LI7000, LiCor Inc.). McGillis *et al.* [2001] found that this contamination resulted in a CO<sub>2</sub> flux bias that was 30% of the true CO<sub>2</sub> flux. The underlying cause of this motion sensitivity is not known, but the behavior is easily replicated. Laboratory experimentation ruled out some potential causes of this behavior including flexing of the optical bench, variations in detector background due to changes in heat transfer associated with changes in orientation, and inertial changes in the rotational speed of the optical chopper. It thus appears likely that the sensitivity arises in the instrument source, as a flexing of the source filament.

[18] The open-path IRGA (LI7500) exhibits much less motion sensitivity than the closed-path sensors (Figure 5). For this reason, only data from the open-path sensor (CO<sub>2</sub> IRGA) were used to compute air-sea CO<sub>2</sub> fluxes. Note that the open-path sensor was converted to a closed-path configuration for this study, as described above. The open-path sensor was not entirely free of motion sensitivity. After correction for the hydrostatic pressure effect described above, a small residual motion-induced signal ( $x_{c,mot}$ ) was found in the converted open-path CO<sub>2</sub> channel. This signal was quantified by a linear regression of the CO<sub>2</sub> signal against the six components of measured platform motion (3 angle rates and 3 linear accelerations) for each flux interval as

$$x_{c,mot} = B_1 a_x + B_2 a_y + B_3 a_z + B_4 r_x + B_5 a_y + B_6 a_z + B_7, \quad (11)$$

where ( $a_x, a_y, a_z$ ) are the 3 linear accelerations and ( $r_x, r_y, r_z$ ) the three angle rates. The motion-related component was

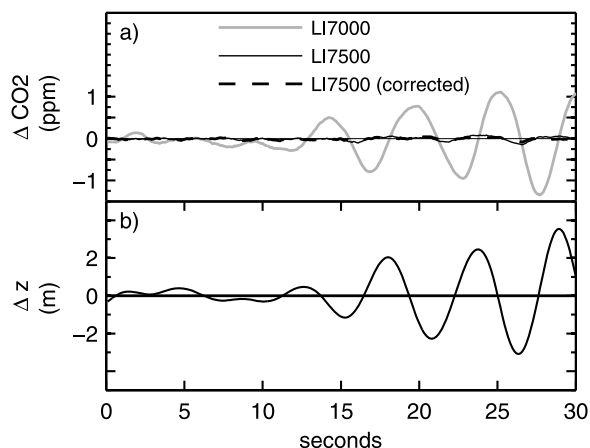


**Figure 5.** (a) Time series from Knorr-07 cruise showing the effect of motion on the CO<sub>2</sub> signal from the LiCor 7000 analyzer (solid light curve), LiCor LI7500 analyzer (solid dark curve), and LiCor LI7500 analyzer corrected for motion sensitivity as described in section 2.4.3 (dashed dark curve). (b) Time series of vertical displacement (meters) of the bow of the R/V *Knorr*. The CO<sub>2</sub> signals were filtered with a 1 s running mean filter to remove high-frequency fluctuations and highlight the ship motion periods.

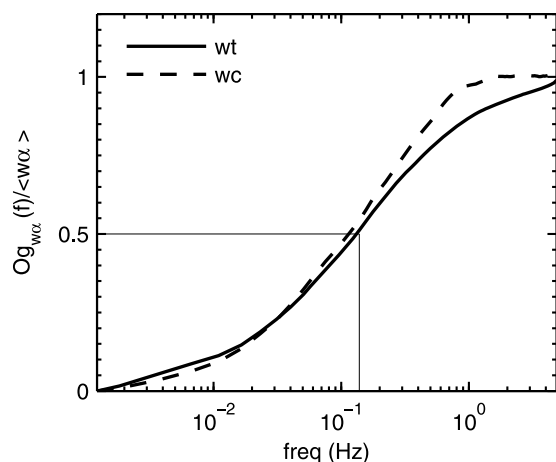


**Figure 6.** Normalized ogives corresponding to fluxes of sensible heat ( $wT$ , solid curve) and carbon dioxide ( $wc$ , dashed curve) measured during the Knorr-07b cruise. Each ogive is the average of 109 13.7 min flux intervals for unstable and neutrally stable atmospheric conditions that were subjectively determined to have high-quality flux cospectra. The line at  $Og_{w\alpha}(f) = 0.5$  (thin solid curve) was used to calculate a correction for the loss of CO<sub>2</sub> fluctuations (and flux) in the sample tube.

subtracted from the CO<sub>2</sub> signal. An example of the motion corrected CO<sub>2</sub> time series from the open-path IRGA is shown in Figure 5 (dashed curve).

#### 2.4.4. Loss of High-Frequency Fluctuations

[19] A key challenge associated with the measurement of air-sea CO<sub>2</sub> flux is that the turbulent CO<sub>2</sub> fluctuations over the ocean are small compared to the noise level of commercially available sensors. Scalar spectral energy densities in the atmospheric surface layer decrease with increasing frequency,  $f$ , according to  $f^{-5/3}$ , such that higher-frequency fluctuations are harder to detect than those at lower frequency. High-frequency fluctuations are also damped as the sample air passes through the inlet tubing to the gas analyzer [Lenschow and Raupach, 1991]. The turbulent eddies corresponding to these scalar fluctuations may therefore not be represented in the calculated flux covariance, and fluxes are underestimated as a result. Tubing losses can be minimized by using short tubing runs and maintaining turbulent airflow in the sample tube, and methods for correcting for flux loss have been developed [Leuning and Moncrieff, 1990].

[20] We addressed high-frequency losses using an ogive method [Marandino *et al.*, 2007]. Similar to other methods for correcting high-frequency loss [e.g., Moore, 1986], the ogive method assumes similarity between the transport of sensible heat and CO<sub>2</sub> in the surface layer. The scalar flux ogives were calculated as  $Og_{w\alpha}(f) = \int_0^f Co_{w\alpha}(f') df'$ , where  $Co_{w\alpha}$  is the cospectrum. Average ogives for sonic temperature and CO<sub>2</sub> flux are shown in Figure 6, normalized by their respective flux covariances. The normalized ogives reveal the distribution of atmospheric eddies that contributed to the measured covariance or flux. Compared with the  $wT$  ogive, assumed to have no high-frequency loss, the ogive for  $wc$  appeared shifted toward lower frequency in Figure 6. This shift is consis-

istent with the loss of high-frequency CO<sub>2</sub> fluctuations and flux, which results in a relative shift in flux-carrying eddies toward lower frequencies. The high-frequency correction was applied for each flux interval by locating a cutoff frequency  $f_c$  at which one half of the  $wT$  covariance was accumulated,  $Og_{wT}(f_c)/\overline{w'T'} = 0.5$  (Figure 6), and assuming that eddies with frequency greater than  $f_c$  made the same relative contribution (50%) to the CO<sub>2</sub> flux. The corrected CO<sub>2</sub> flux was calculated as  $\overline{w'c'}_{corr} = 2 Og_{wc}(f_c)$ . The results of this correction procedure were not sensitive to the selection of the cutoff frequency. The average variation in the CO<sub>2</sub> flux was only 3% when accumulated flux fractions ranging from 0.4 to 0.7 were used.

#### 2.5. Effects of Flow Distortion

[21] There is no generally accepted method for modeling or correcting for the effects of flow distortion. Studies have demonstrated that the effect of flow distortion on scalar fluxes is small compared to the momentum fluxes. Pedreros *et al.* [2003] found that "...the results for heat flux do not appear to be contaminated by turbulent flow distortion." Since CO<sub>2</sub> is a scalar, it is likely that flow distortion effects on the CO<sub>2</sub> flux would be similar to the heat flux contamination (very small), rather than the momentum flux contamination. Yelland *et al.* [2002] modeled flow distortion about the R/V *Knorr*, and found that effects at the bow mast were relatively small (about 2% acceleration). The resulting uncertainty is small compared with other sources of uncertainty in our measurements.

[22] The methodology used in all previous air-sea gas flux measurements has been to limit the range of relative wind directions. In our analysis, we followed this same approach. The relative wind direction criteria used by McGillis *et al.* [2001] was  $\pm 60$  degrees of the bow, while Blomquist *et al.* [2006] used  $\pm 120$  degrees, and Marandino *et al.* [2007] used  $\pm 60$  degrees. We used a 60 degree criterion for the quadrant in which the other sonic anemometer is mounted, and a 90 degree criterion in the quadrant that has no obstruction from other sensors. Our range of wind directions lies within the range of the previous studies.

#### 2.6. Seawater pCO<sub>2</sub>

[23] The CO<sub>2</sub> concentration in seawater was measured continuously in the ship's wet laboratory using two separate equilibrator systems. In each system, air was equilibrated with seawater from the ship's uncontaminated seawater supply, and recirculated in a closed loop through an IRGA. The first system used a membrane-based gas/liquid contactor (LiquiCell X40) with an LI7000 closed-path IRGA (LiCor, Inc.). This equilibrator was deployed during both Knorr-07a and Knorr-07b cruises. The second system was a homemade showerhead-type equilibrator and an LI820 closed-path IRGA (LiCor, Inc.). This equilibrator was deployed only during the Knorr-07b cruise. Seawater pCO<sub>2</sub> measured by the two systems showed excellent agreement (linear regression slope 1.02,  $r^2 = 0.99$ ).

#### 2.7. Data Processing and Quality Control

[24] Turbulence data from the sonic anemometer, motion sensor, and CO<sub>2</sub> and H<sub>2</sub>O IRGAs in the bosun locker were sampled at 10 Hz and archived in 1 h data files. The data processing steps are summarized in Figure 7. The measured

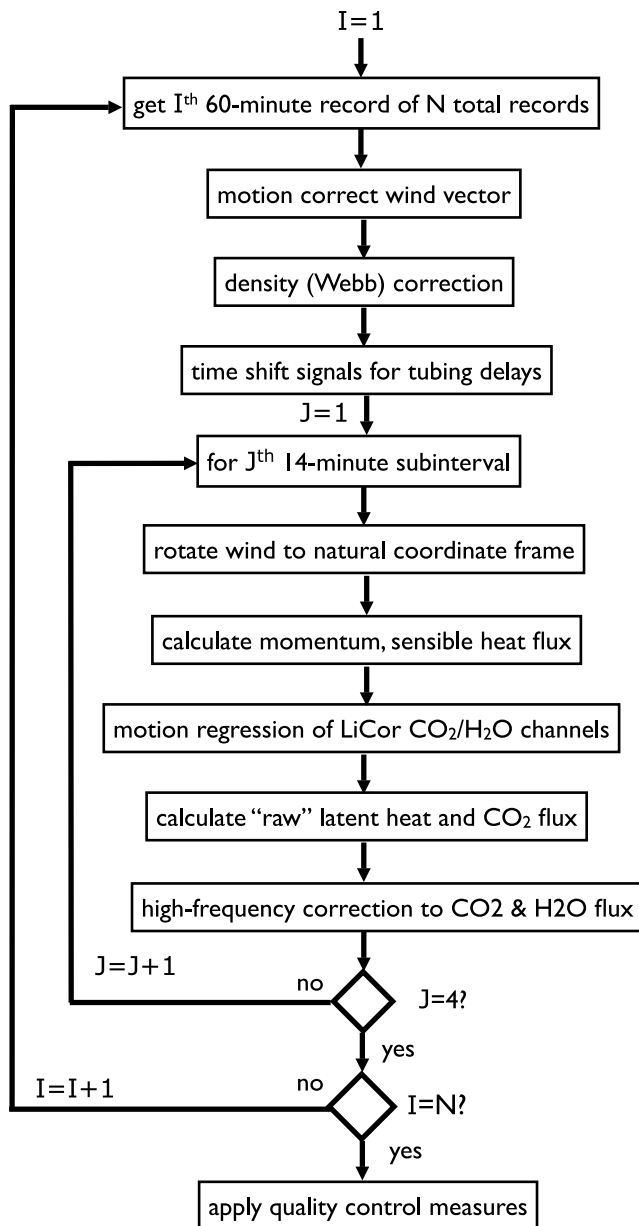


Figure 7. Data processing flow diagram.

wind vector was corrected for platform motion using the motion signals and GPS data following *Miller et al.* [2008]. The IRGA signals were time shifted to account for the 1.2 s time delay due to travel time in the sample tube. The first and last 160 s of the 1 h time series were removed to eliminate edge effects of digital filters used for the platform motion corrections. The remaining  $\sim 55$  min time series was divided into four 13.7 min subintervals (8192 10 Hz samples) for calculating fluxes. For each subinterval, the wind vector was rotated into a ‘natural’ coordinate frame, with a nonzero along-wind component and zero-mean cross-wind and vertical velocity components. The corrected winds and scalars were used to calculate the turbulent fluxes according to equations (2)–(5), and the H<sub>2</sub>O and CO<sub>2</sub> fluxes were corrected for high-frequency flux losses as described previously.

[25] The quality of the measured CO<sub>2</sub> fluxes was first evaluated using objective criteria. Fluxes were rejected due to instrument malfunction of the sonic anemometer, motion sensor, IRGAs, or pressure sensor during each 13.7 min flux interval. Intervals were also rejected when the mean wind direction relative to the ship over the flux interval was  $>90^\circ$  from forward ( $>60^\circ$  for the quadrant with the adjacent sonic). Stationarity of the CO<sub>2</sub> flux was assessed by comparing the 13.7 min flux and the average flux of four 2048 sample (3.4 min) subintervals. Following *Foken and Wichura* [1996], intervals were rejected if the difference was greater than 30%. A second, subjective approach was also used for quality control. This approach involved examining the flux cospectra for momentum, sensible and latent heat, and CO<sub>2</sub> for each 13.7 min flux interval. The theoretical-empirical Kaimal cospectral shape [*Kaimal et al.*, 1972] was also plotted, and a subjective decision was made as to whether the  $wc$  flux cospectrum was similar to the other scalar cospectra and the Kaimal cospectrum.

[26] Since the high-frequency correction was dependent upon the flux cospectra and ogives, only intervals that passed the subjective quality control test were considered to have valid estimates of the high-frequency correction. For intervals that did not pass the subjective quality control test, average correction factors (gains) calculated for the fluxes during periods that did pass the test were used. Separate gains were calculated for CO<sub>2</sub> and H<sub>2</sub>O, and for unstable ( $z/L < 0$ ) and stable ( $z/L > 0$ ) atmospheric conditions, where  $z$  is the measurement height,  $L = -\bar{\theta}_v u_*^3 / K g w' \theta'_v$  is the Obhukov length,  $\theta_v$  is the virtual potential air temperature,  $u_*$  is the friction velocity,  $K = 0.4$  is the von Karman constant, and  $g$  is gravity. For unstable conditions during Knorr-07b, the median CO<sub>2</sub> flux loss was 13%, while the H<sub>2</sub>O flux loss was 34%. The greater attenuation of water vapor fluctuations is consistent with previous studies. For example, *Ibrom et al.* [2007] found a 40% loss of water vapor flux compared to a 4% loss of CO<sub>2</sub> flux, which they hypothesize was due to interactions between the water vapor and walls of the tubing. During stable conditions, the flux loss for both CO<sub>2</sub> (26%) and H<sub>2</sub>O (82%) was larger than for unstable conditions. The increase in flux loss during stable conditions is consistent with the shift of the flux toward higher frequency (smaller) eddies during stable conditions, since tubing losses are greater for high frequency fluctuations.

### 3. Results and Discussion

[27] A total of 526 h of data were collected, including 326 h during Knorr-07a and 200 h during Knorr-07b. Since each hour was divided into four subintervals, there were a total of 2104 flux intervals. The results of the quality control tests are summarized in Table 1. For the combined data set, 429 of the intervals (20%) passed objective quality tests related to the turbulent flux measurement (system up and sampling, sufficient pump flow, no instrument spikes, acceptable wind direction, and  $w'c'$  stationarity), with a high percentage (65%) of the intervals failing the stationarity test. Fewer intervals (9%) passed subjective inspection of the flux cospectra, and only 73 intervals passed both the objective and subjective quality tests. The fact that many intervals failed the stationarity test (Table 1) was surprising,

**Table 1.** CO<sub>2</sub> Flux Quality Control

	Knorr-07a Barbados–Iceland	Knorr-07b Iceland–WHOI	Combined Cruises
Days at sea	14	10	24
Hours of data collected	326	200	526
13.7 min flux intervals	1304	800	2104
Objective quality controls intervals passed			
Condition 1: system up/no instrument spikes	752	412	55%
Condition 2: acceptable wind direction	853	791	78%
Condition 3: $w'x'_c$ stationary	442	287	35%
Conditions 1–3 satisfied	253	176	20%
Subjective QC (inspection of cospectra)	82	109	9%
Conditions 1–3 satisfied, and subjective QC	25	48	3%
Air-sea pCO <sub>2</sub> difference > 40 ppm	354	607	46%

since the flux interval length of 14 min was relatively short. This was potentially due to small background changes in CO<sub>2</sub> concentration (heterogeneity), or due to low-frequency sensor drift.

### 3.1. Meteorology and Heat Fluxes

[28] Wind speed at 10 m height was low to moderate throughout the Knorr-07 cruises, averaging 6 m s<sup>-1</sup> for Knorr-07a and 7 m s<sup>-1</sup> for Knorr-07b (range of 1–15 m s<sup>-1</sup>, Figure 8a). During Knorr-07a, south of 45°N, sea surface temperature (SST) was higher than air temperature (Figure 8b), with upward sensible and latent heat fluxes averaging 41 and 110 Wm<sup>-2</sup>, respectively. North of 45°N, the air-sea temperature difference was small, and the total heat flux averaged 16 Wm<sup>-2</sup>. For this cruise, the atmosphere was unstable ( $z/L < -0.07$ ) for 64% of intervals, stable ( $z/L > 0.07$ ) for 4% of intervals, and neutral for 32% of intervals. During Knorr-07b, the average air temperature was warmer than SST, with negative (downward) sensible and latent heat fluxes (average -24 and -7 Wm<sup>-2</sup>, respectively, Figure 8c). For this cruise, the atmosphere was unstable for 17% of intervals, stable for 40% of intervals, and neutral for 43% of intervals. Fog conditions during stable periods resulted in higher rates of data loss, presumably due to condensation in the sample lines. For each flux interval, the correlation between the sonic temperature and the H<sub>2</sub>O IRGA water vapor signal was examined for a range of sample shifts to determine the tubing delay. During unstable conditions the relationship showed a clear maximum which was used as an empirical estimate of the tubing delay. During stable conditions, there was frequently no clear maximum in the correlation, which we believe was due to condensation in the sample lines, as the stable conditions often corresponded to the presence of fog.

### 3.2. Air and Seawater pCO<sub>2</sub>

[29] Atmospheric pCO<sub>2</sub> was relatively constant during each cruise, 387 ± 4 ppm for Knorr-07a and 377 ± 4 ppm for Knorr-07b (Figure 8d). Sea surface pCO<sub>2</sub> was mostly undersaturated with respect to the atmosphere. This was presumably a result of biological production, as chlorophyll levels were relatively high (Figure 8d). During the last part of Knorr-07b, along the North American continental shelf, seawater pCO<sub>2</sub> was supersaturated with respect to atmospheric levels (Figure 8d). The mean water-air pCO<sub>2</sub> difference was -49 ± 22 ppm during undersaturated periods north of 39°N, and 43 ± 28 ppm in the supersaturated

region. Overall, less than half (46%) of the intervals had an air-sea pCO<sub>2</sub> difference greater than 40 ppm (Table 1).

### 3.3. Atmospheric CO<sub>2</sub> Fluctuations

[30] The standard deviation of CO<sub>2</sub> fluctuations ( $\sigma_c$ ) measured by the CO<sub>2</sub> IRGA during Knorr-07b was ~0.13 ppm, comparable to the manufacturer's root-mean square (RMS) noise specification of 0.11 ppm for 10 Hz sample rate (Figure 9). However, atmospheric CO<sub>2</sub> fluctuations were expected to be much smaller. An estimate of the expected  $\sigma_c$  was obtained using a simple neutral surface layer scaling,  $F_c = C_1 \sigma_w \sigma_c$  with  $C_1 = 0.4$ , analogous to relationships used for other scalars [Stull, 1988]. For this estimate, the CO<sub>2</sub> flux  $F_c$  was calculated according to equation (1), using the parameterization of Wanninkhof [1992] to estimate the piston velocity, and the Knorr-07b measured air-sea pCO<sub>2</sub> difference, wind speed, and standard deviation of vertical wind,  $\sigma_w$  (Figure 9). This calculation suggests much smaller CO<sub>2</sub> fluctuations ( $\sigma_c \sim 0.05$  ppm or less, open circles) than those measured (open squares). The difference between the measured and expected  $\sigma_c$  magnitude and the similarity between the measured  $\sigma_c$  and the manufacturer's noise specification suggests that the sample-to-sample CO<sub>2</sub> fluctuations mostly reflected the sensor noise and not the true atmospheric CO<sub>2</sub> fluctuations.

[31] The sensor noise levels shown in Figure 9 were also found in the CO<sub>2</sub> power spectra. Measured CO<sub>2</sub> and H<sub>2</sub>O power spectral densities ( $S_\alpha(f)$ ) are shown in Figure 10, along with theoretical-empirical surface-layer relationships ("Kaimal" spectra) calculated as  $f S_\alpha(f) = \alpha_*^2 \gamma_\alpha / (2\pi K)^{2/3} \phi_\epsilon^{-1/3} \phi_h(fz/\bar{U})^{-2/3}$ , where  $f$  is frequency,  $\alpha_* = -w'\alpha'/u_*$  is the turbulent CO<sub>2</sub> or H<sub>2</sub>O scale,  $\gamma_\alpha$  is a constant (assumed 0.8),  $K$  is the von Karman constant (0.4),  $\phi_\epsilon = (1 + 0.5|z/L|^{2/3})^{3/2}$  and  $\phi_h = (1 + 16|z/L|)^{-1/2}$  are the stability functions for dissipation and heat flux, and  $\bar{U}$  is the mean wind speed [Kaimal et al., 1972]. The Knorr-07b measurements of  $\bar{U}$ ,  $u_*$ ,  $w'q'$ , and  $z/L$  were used to calculate the Kaimal spectra. The turbulent CO<sub>2</sub> scale  $c_*$  was estimated from the CO<sub>2</sub> flux calculated from equation (1). The measured water vapor power spectrum shape and magnitude were similar to the Kaimal spectrum between ~0.02–0.2 Hz (Figure 10a). In contrast, the measured CO<sub>2</sub> power spectrum was several times larger than the Kaimal spectrum (Figure 10b). At frequencies larger than 0.1 Hz, the measured CO<sub>2</sub> power spectra increased, whereas the Kaimal spectrum decreased. The behavior of the CO<sub>2</sub> spectrum is consistent with a noise-

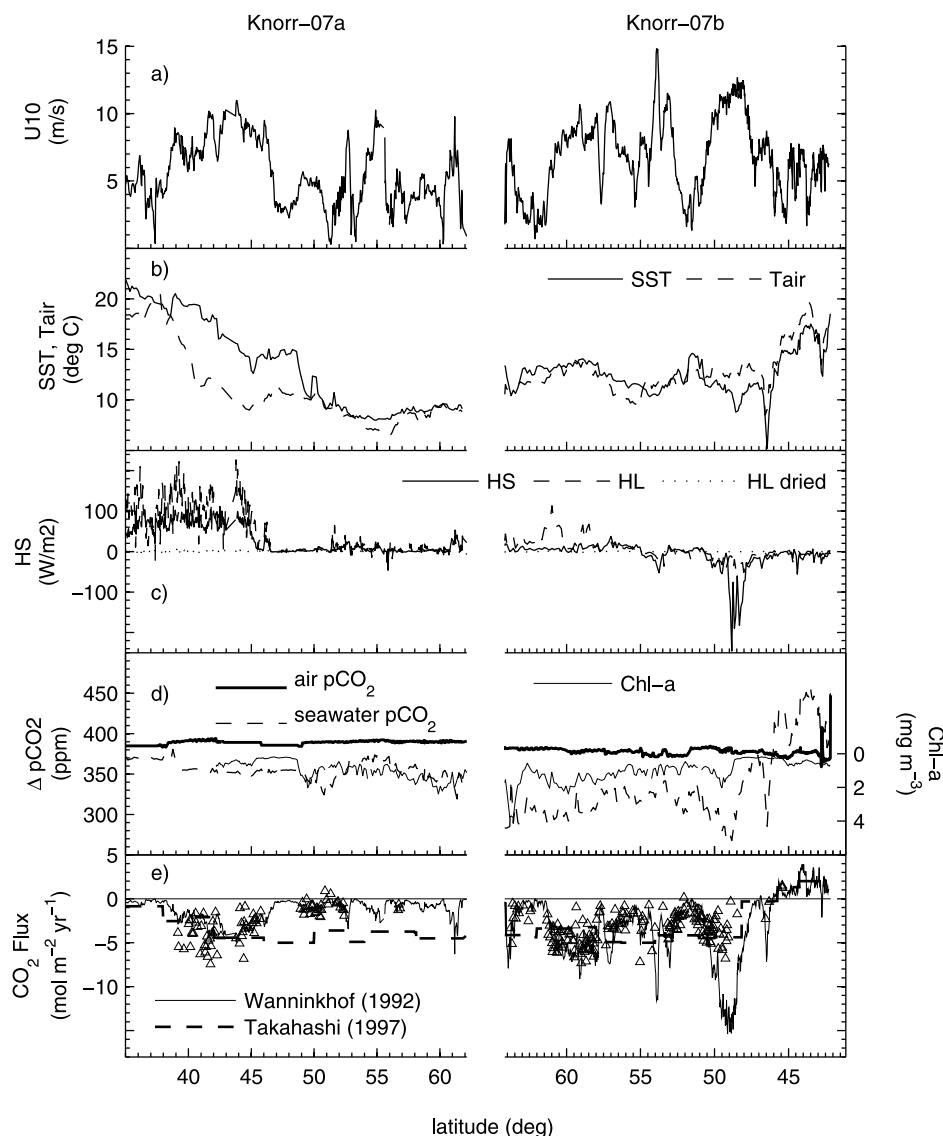


**Figure 8.** Summary of Knorr-07 cruises. (left) Latitude increasing: Bridgetown, Barbados, to Reykjavik, Iceland (29 May to 9 June). (right) Latitude decreasing: Reykjavik, Iceland, to Woods Hole, Massachusetts (17–26 July). (a) Wind speed at 10 m height ( $\text{m s}^{-1}$ ); (b) SST ( $^{\circ}\text{C}$ , solid curve) and air temperature ( $^{\circ}\text{C}$ , dashed curve); (c) sensible heat flux (solid curve), latent heat flux (dashed curve), and effective latent heat flux measured by the CO<sub>2</sub> IRGA downstream of the Nafion drier (dotted curve); (d) air (solid thick curve) and seawater (dashed curve) pCO<sub>2</sub> (ppm), and MODIS chlorophyll ( $\text{mg m}^{-3}$ , solid thin curve) plotted on a reverse axis using (left) the 17 May to 17 June 2007 image and (right) the July 2007 monthly image; and (e) air-sea flux of CO<sub>2</sub> ( $\text{mol CO}_2 \text{ m}^{-2} \text{ yr}^{-1}$ , triangles) along with CO<sub>2</sub> flux estimated using equation (1) and the parameterization of Wanninkhof [1992] (solid curve). Also shown is the CO<sub>2</sub> flux along the cruise track from the climatology of Takahashi *et al.* [1997] (thick dashed curve).

dominated signal at frequencies above 0.1 Hz. At frequencies less than 0.1 Hz, neither the CO<sub>2</sub> nor H<sub>2</sub>O power spectrum showed inertial range behavior (Figure 10b).

[32] To resolve CO<sub>2</sub> fluxes, the IRGA must therefore be capable of measuring CO<sub>2</sub> fluctuations much smaller than the sensor's RMS noise specification. The covariance (cospectra) between CO<sub>2</sub> and vertical wind used to calculate fluxes (flux cospectra) served as a noise filter since the CO<sub>2</sub> signal noise was uncorrelated with  $w$ . This is demonstrated by the  $wc$  and  $wT$  flux cospectra (Figure 11). Except for

frequencies above 1 Hz where the CO<sub>2</sub> flux was attenuated by tubing loss, the  $wc$  and  $wT$  cospectra were similar. The  $wc$  and  $wT$  cospectral shapes were also similar to the Kaimal cospectrum (note: the Kaimal cospectra in Figure 11 are for neutral stability, and were not frequency-shifted to account for stability effects). These cospectra indicate that the true atmospheric CO<sub>2</sub> fluctuations were detected by the CO<sub>2</sub> IRGA, even though they were masked by instrumental noise.

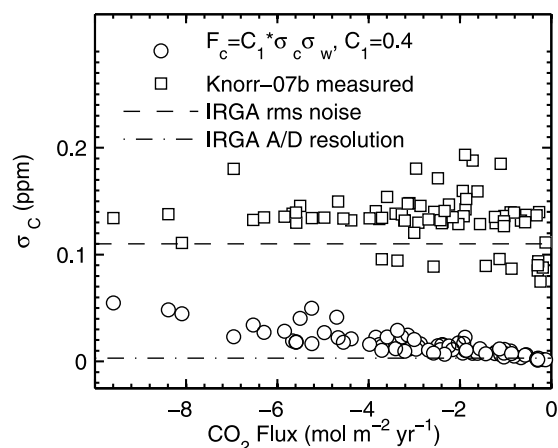


**Figure 9.** Standard deviation of atmospheric CO<sub>2</sub> fluctuations (ppm) versus CO<sub>2</sub> flux (mol CO<sub>2</sub> m<sup>-2</sup> yr<sup>-1</sup>). The CO<sub>2</sub> flux was estimated using equation (1) and the measured air-sea pCO<sub>2</sub> difference, wind speed, and the piston velocity parameterization of Wanninkhof [1992] during Knorr-07b. The measured  $\sigma_c$  is shown as open squares. An estimate of  $\sigma_c$  calculated using a simple surface layer scaling relationship described in the text is shown as open circles. Also shown are the manufacturer's specified RMS noise level of the LI7500 IRGA at 10 Hz (dashed curve), and the estimated resolution of the IRGA A/D conversion (dash-dotted curve).

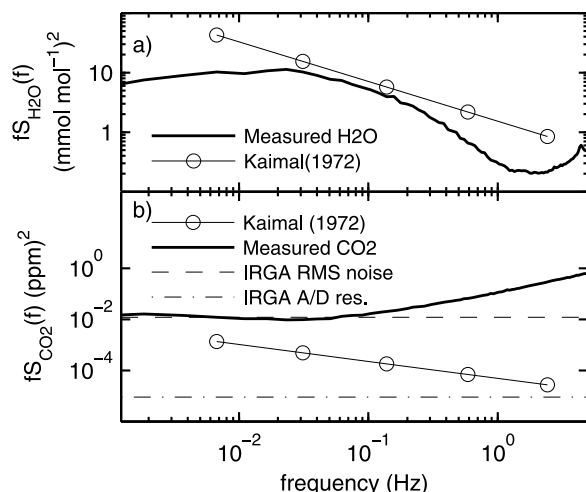


**Figure 10.** Frequency-weighted power spectra,  $fS(f)$  of (a) water vapor (mmol<sup>2</sup> mol<sup>-2</sup>) and (b) carbon dioxide (ppm<sup>2</sup>) measured during Knorr-07b (thick solid curves). The Kaimal *et al.* [1972] power spectra are shown as solid curves with circles, calculated as described in the text. The spectra are the average of 109 13.7 min flux intervals for unstable and neutrally stable atmospheric conditions. The RMS noise level of the LiCor LI7500 CO<sub>2</sub> channel is shown in Figure 10b as the dashed curve, and the estimated resolution of the IRGA A/D conversion is shown as the dash-dotted curve. The RMS noise level of the IRGA water vapor channel is several orders of magnitude below the y axis scale minimum, and therefore is not shown.

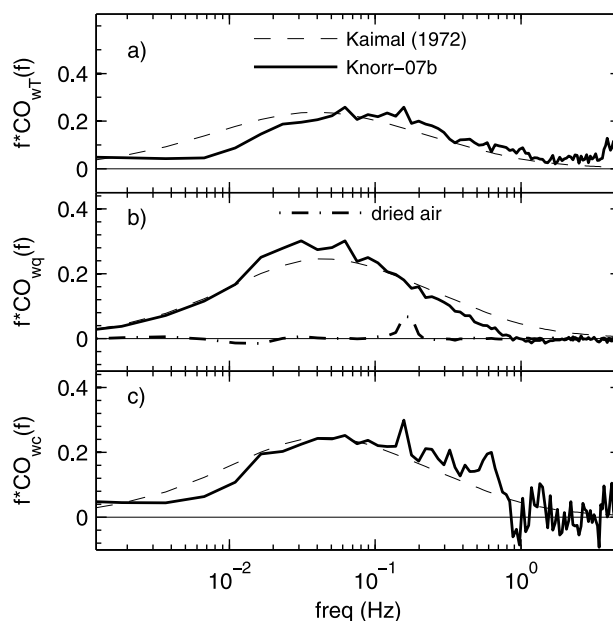


**Figure 11.** Normalized flux cospectra for (a) sensible heat,  $wT$ ; (b) latent heat,  $wq$ ; and (c) carbon dioxide,  $wc$ . The cospectra are the average of 109 13.7 min flux intervals for unstable and neutrally stable atmospheric conditions. Measured cospectra are shown as solid curves, and Kaimal *et al.* [1972] cospectra are shown as dashed curves. The  $wq$  cospectrum measured by the CO<sub>2</sub> IRGA downstream of the Nafion drier is shown as the dash-dotted curve in Figure 11b.

[33] The  $wc$  cospectra provide strong evidence that air-sea CO<sub>2</sub> fluxes were resolved in our measurements. The similarity between the  $wc$  and  $wT$  cospectra was not an artifact of the Webb correction for water vapor since the sample stream was dried and the  $wq$  cospectrum of the dried air stream was essentially zero (Figure 11b, dash-dotted curve). Similarly, our laboratory tests (not shown) and similar tests by LiCor (George Burba, personal communication, 2009) indicate that even short runs (2 m) of tubing are sufficient to eliminate temperature fluctuations at the IRGA, provided the tubing walls are conductive (we used aluminum-lined tubing). Furthermore, Figures 3c and 3f show that pressure fluctuations were largely unaffected by the Nafion tubing bundle. The similarity between the  $wc$  cospectrum and both the measured  $wT$  cospectrum and the theoretical-empirical surface layer cospectrum supports that the true CO<sub>2</sub> flux was resolved by the system.

[34] These results suggest that the IRGA was capable of resolving CO<sub>2</sub> fluctuations in the atmosphere below its RMS noise level. The CO<sub>2</sub> signal quantization associated with the analog-to-digital (A/D) conversion of the detector output provides a lower limit (i.e., best-case scenario) of the IRGA resolution. The sensor uses a 16-bit A/D converter, and the CO<sub>2</sub> signal is oversampled and averaged, providing an effective A/D resolution of 19 bits at 10 Hz (G. Burba, personal communication, 2009). For the CO<sub>2</sub> absorbance range of the LI7500, this yields a resolution of approximately 0.003 ppm. This limit is indicated in Figures 9 and 10 (horizontal dash-dotted curves). Assuming this limit represents the effective CO<sub>2</sub> resolution, Figures 9 and 10

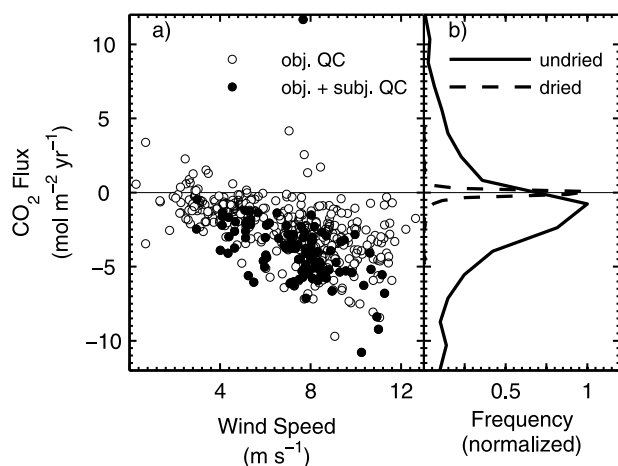


**Figure 12.** (a) CO<sub>2</sub> flux (mol CO<sub>2</sub> m<sup>-2</sup> yr<sup>-1</sup>) versus 10 m wind speed (m s<sup>-1</sup>) measured on Knorr-07 cruises. All of the points passed objective quality control tests, and solid circles indicate intervals that also passed subjective inspection of cospectra. (b) Histogram of the Webb correction term (mol CO<sub>2</sub> m<sup>-2</sup> yr<sup>-1</sup>) for CO<sub>2</sub> flux due to the latent heat flux for the dried sample air stream (dashed curve), and which would have been necessary if the sample air stream had not been dried (solid curve).

suggest that the IRGA is capable of measuring fluxes over most of the conditions encountered during the Knorr-07 cruises. This reasoning assumes that all sources of sensor noise (due to temperature sensitivity, drift, etc.) are uncorrelated with the vertical wind. The true effective sensor resolution to CO<sub>2</sub> fluctuations presumably lies somewhere between the sensor's RMS noise level and the A/D resolution (i.e., between the dashed and dash-dotted curves in Figures 5 and 6).

### 3.4. Air-Sea CO<sub>2</sub> Flux

[35] The turbulent CO<sub>2</sub> fluxes calculated using the port-side and starboard side sonic anemometers showed good agreement. A linear regression of the fluxes calculated using the two anemometers was 0.93, and the  $r^2$  statistic was 0.87. The CO<sub>2</sub> flux during the Knorr-07 cruises was generally from the atmosphere to the ocean (negative), consistent with the water-air partial pressure difference (Figures 8d and 8e). The flux magnitude increased with wind speed (Figure 12a), and was in broad agreement with the gas exchange parameterization of *Wanninkhof* [1992] (Figure 8e). The average air-to-sea CO<sub>2</sub> flux of the 429 intervals that passed quality control was  $-3.1 \pm 0.1$  mol CO<sub>2</sub> m<sup>-2</sup> yr<sup>-1</sup>. For comparison, the CO<sub>2</sub> flux along the Knorr-07 cruise tracks was extracted from the monthly CO<sub>2</sub> flux climatology of *Takahashi et al.* [1997], using the month of June for Knorr-07a and July for Knorr-07b (Figure 8e, dashed curve). For both cruises, the mean CO<sub>2</sub> flux from the climatology was  $-2.3$  mol CO<sub>2</sub> m<sup>-2</sup> yr<sup>-1</sup>. Some features of the climatology were seen in the measured and calculated fluxes. During Knorr-07a, both the climatology and calculated CO<sub>2</sub> flux showed a marked transition from near-zero to higher (negative) fluxes between 38 and 40°N (Figure 8e). During Knorr-07b, the climatology and calculated fluxes showed a change from

CO<sub>2</sub> uptake to emission as the ship crossed into waters along the North American continental shelf.

[36] The removal of water vapor fluctuations in the CO<sub>2</sub> IRGA sample cell with the Nafion drier almost completely eliminated the Webb correction. The average latent heat flux magnitude measured by the H<sub>2</sub>O IRGA upstream of the Nafion drier was 48 Wm<sup>-2</sup>. In contrast, the average latent heat flux magnitude measured by the CO<sub>2</sub> IRGA downstream of the Nafion drier was only 1.2 Wm<sup>-2</sup> (e.g., Figure 8c). The use of the drier therefore resulted in a 97% reduction in both the latent heat flux and the Webb correction for water vapor, which scales linearly with latent heat flux (equation (6) and Figure 12b). The average Webb correction to the CO<sub>2</sub> flux for the undried air stream was 13 mol CO<sub>2</sub> m<sup>-2</sup> yr<sup>-1</sup>, more than 4 times the average CO<sub>2</sub> flux magnitude. In contrast, the Webb correction for the dried air stream measured by the CO<sub>2</sub> IRGA averaged only 0.26 mol CO<sub>2</sub> m<sup>-2</sup> yr<sup>-1</sup>, or 8% of the average CO<sub>2</sub> flux.

[37] The correction for the loss of high-frequency flux due to tubing attenuation was small and, as expected, increased the magnitude of the flux (Figure 13). In contrast, the motion contamination of the wind vector and the sensitivity of the IRGA CO<sub>2</sub> channel to platform motion were large, and their impacts differed between the two Knorr-07 cruises. The motion contamination of the wind vector resulted in more positive CO<sub>2</sub> fluxes for both cruises, and its magnitude was large enough to change the sign of the measured flux during Knorr-07a. The motion sensitivity of the IRGA resulted in a more negative CO<sub>2</sub> flux during Knorr-07a and a more positive CO<sub>2</sub> flux during Knorr-07b. We did not find a simple relationship between the size and

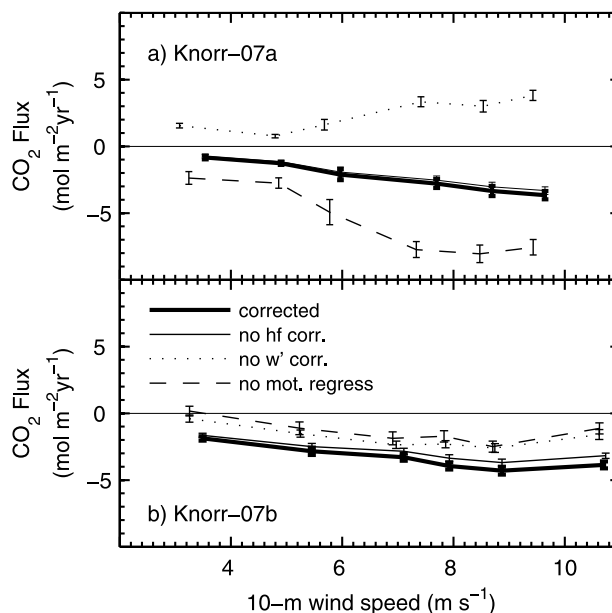


**Figure 13.** Bin-averaged CO<sub>2</sub> flux (mol CO<sub>2</sub> m<sup>-2</sup> yr<sup>-1</sup>) versus 10 m wind speed (m s<sup>-1</sup>) showing the impact of different flux corrections for (a) Knorr-07a and (b) Knorr-07b: corrected fluxes (thick solid curve), without high-frequency correction (thin solid curve), without vertical wind correction for platform motion (dotted curve), and without motion regression applied to open-path IRGA (dashed curve). Error bars are standard error.

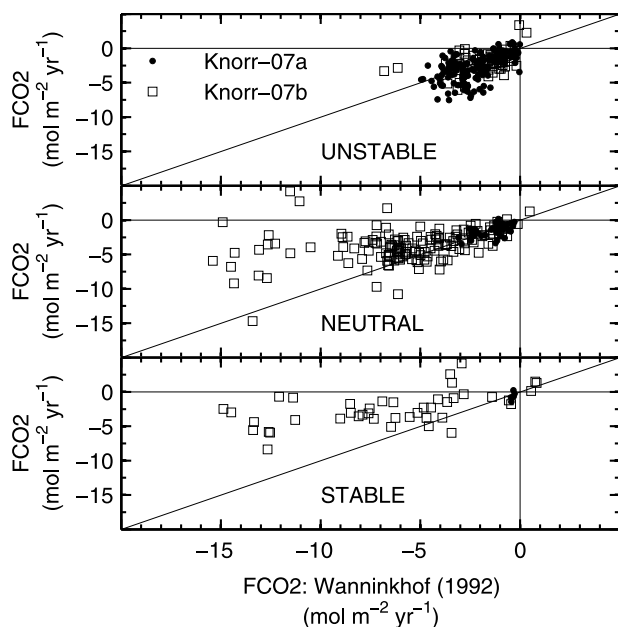


**Figure 14.** Measured CO<sub>2</sub> flux ( $\text{mol CO}_2 \text{ m}^{-2} \text{ yr}^{-1}$ ) versus CO<sub>2</sub> flux calculated from equation (1) using the parameterization of *Wanninkhof* [1992] ( $\text{mol CO}_2 \text{ m}^{-2} \text{ yr}^{-1}$ ) for different atmospheric stratification: (top) unstable, (middle) neutral, and (bottom) stable. Knorr-07a cruise data are shown as solid points, and Knorr-07b data are shown as open squares. Diagonal curves represent 1:1 lines.

sign of these corrections and cruise conditions (e.g., wind direction relative to ship), suggesting that the corrections may be dependent on complicated interactions between the ship motion and wind and wavefields.

[38] The CO<sub>2</sub> fluxes measured during the Knorr-07 cruises are compared with estimates calculated using equation (1) for different atmospheric stabilities in Figure 14. The difference between the measured and calculated fluxes exhibited atmospheric stability-dependent behavior. During unstable conditions, the measured and calculated fluxes showed good agreement (Figure 14, top). Neutrally stable cases showed good agreement for flux magnitudes less than  $5 \text{ mol CO}_2 \text{ m}^{-2} \text{ yr}^{-1}$ ; but, for higher flux magnitudes, the measured fluxes were less than calculated fluxes (Figure 14, middle). For stable atmospheric conditions, the magnitude of the measured fluxes was lower than the computed fluxes (Figure 14, bottom). During stable conditions and during high winds, the proportion of the turbulent flux at high frequency increases. The underestimation of the measured flux during these conditions could therefore have resulted from high-frequency losses that were not adequately corrected by the procedure described previously. Further measurements are needed to assess the system performance during stable atmospheric conditions.

### 3.5. Piston Velocity

[39] The measured CO<sub>2</sub> flux and air-sea pCO<sub>2</sub> difference were used to calculate the piston velocity according to equation (1). Sea surface pCO<sub>2</sub> was related to the bulk air concentration ( $C_a$ ) by Henry's Law,  $C_a/\alpha$ , where  $\alpha$  is the dimensionless solubility. The computed gas transfer coefficients were normalized to a Schmidt number ( $=\nu/D$ ,

where  $\nu$  is the kinematic viscosity and  $D$  is the molecular diffusivity) of 660 assuming  $Sc^{-1/2}$  dependence. Piston velocities were rejected when the air-water pCO<sub>2</sub> difference was less than 35 ppm, and data collected during Knorr-07a south of 39°N were rejected due to problems with the equilibrator. The measured piston velocities increased with wind speed and were broadly consistent with the parameterizations shown in Figure 15. Below  $4 \text{ m s}^{-1}$ , the measured  $k$  was mostly higher than the parameterizations. Reasonable values of the piston velocity were obtained during the few periods that passed the objective quality control tests and had positive CO<sub>2</sub> flux (from ocean to atmosphere).

[40] For the downward CO<sub>2</sub> flux periods, the individual piston velocity measurements in Figure 15 were denoted with numbers 1–10 according to the deciles of CO<sub>2</sub> flux magnitude encountered during the Knorr-07 cruises. Due to the behavior of the measured fluxes during neutral and stable conditions (Figure 14), only unstable conditions are included in Figure 15. Plausible piston velocities were obtained even in the lowest decile bin, when CO<sub>2</sub> fluxes were small (magnitude less than  $0.6 \text{ mol CO}_2 \text{ m}^{-2} \text{ yr}^{-1}$ , Figure 15, points marked with “1”). This suggests that the flux system was capable of resolving small CO<sub>2</sub> fluxes. While these results do not provide a precise estimate of the resolution of the CO<sub>2</sub> flux measurement, it appears that reasonable fluxes were measured over the range of fluxes encountered during unstable atmospheric conditions on the Knorr-07 cruises.

### 3.6. Global Estimate of the CO<sub>2</sub> Flux Measurement Capability by Eddy Covariance

[41] The approach taken in this study, primarily the reduction in Webb correction by drying the air stream, resulted in a significant improvement in the signal-to-noise ratio of the air-sea CO<sub>2</sub> flux measurement. This improve-

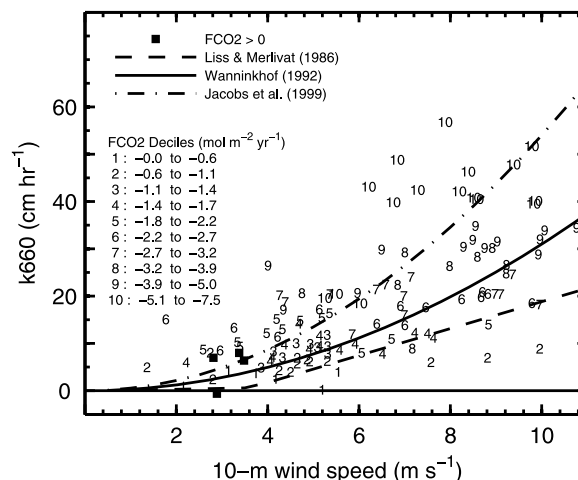


**Figure 15.** Piston velocity ( $\text{cm hr}^{-1}$ ) versus 10 m wind speed for  $Sc = 660$  for the Knorr-07 cruises. Upward (sea-to-air) CO<sub>2</sub> fluxes shown as solid squares. Downward fluxes shown as numbers 1–10, corresponding to deciles of CO<sub>2</sub> flux magnitude. Also shown are parameterizations of *Liss and Merlivat* [1986] (dashed curve), *Wanninkhof* [1992] (solid curve), and *Jacobs et al.* [1999] (dash-dotted curve).

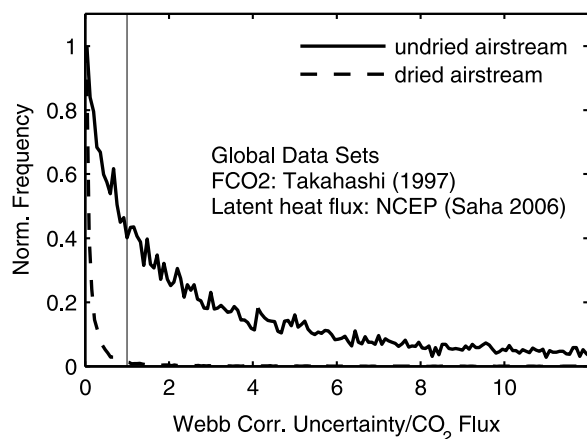


**Figure 16.** Global estimate of the uncertainty in the air-sea CO<sub>2</sub> flux due to the uncertainty in the latent heat flux portion of the Webb correction (i.e., for closed-path eddy covariance systems), plotted as the ratio of the Webb correction uncertainty magnitude to the true air-sea CO<sub>2</sub> flux magnitude for an undried (solid curve) and for a simulated dried air stream (dashed curve). Global CO<sub>2</sub> flux climatology is from *Takahashi et al.* [1997], and latent heat flux climatology is from *Saha et al.* [2006]. Drying of the air stream was assumed to eliminate 97% of the water vapor fluctuations (and flux; see Figure 8). Uncertainty in the air-sea latent heat flux measurement by eddy covariance systems was assumed to 20%. Ratios greater than one indicate correction uncertainties larger than the actual flux.

ment potentially enables air-sea CO<sub>2</sub> flux measurements to be made over much more of the ocean than previously possible. We demonstrate this by combining the monthly global ocean CO<sub>2</sub> flux climatology [*Takahashi et al.*, 1997] and the NCEP daily latent heat flux climatology for 2008 [*Saha et al.*, 2006] interpolated to the same spatial (1° × 1°) resolution and averaged to a monthly time step. A Webb correction “climatology” was calculated from the latent heat flux climatology, assuming a closed-path CO<sub>2</sub> flux system with no temperature fluctuations in the IRGA cell. The ratio of the uncertainty in the latent heat flux Webb correction to the CO<sub>2</sub> flux is shown in Figure 16 for dried and undried air streams. The dried air sample latent heat flux was estimated assuming a 97% reduction of the climatological latent heat flux (Figure 12b). The Webb correction uncertainty for both undried and dried cases was estimated assuming the uncertainty of the air-sea latent heat flux was 20%.

[42] When the ratio is greater than 1, the uncertainty in the Webb correction is larger than the actual CO<sub>2</sub> flux. Drying the air stream markedly reduces the uncertainty in the Webb correction and therefore in the CO<sub>2</sub> flux. Drying therefore should enable more accurate measurements of CO<sub>2</sub> flux due to a reduction in the measurement uncertainties. For the undried sample stream, the *uncertainty* in CO<sub>2</sub> flux due to the uncertainty in the latent heat flux Webb correction was larger than the climatological CO<sub>2</sub> flux for roughly 70% of the pixels (Figure 16, solid curve). By contrast, the dried case exhibits a dramatic reduction in the Webb correction, with only 9% of the pixels showing an

uncertainty due to the Webb correction equal to or greater than the CO<sub>2</sub> flux. (Figure 16, dashed curve). This estimate suggests that by drying the air stream, a much greater ocean area may be amenable to direct covariance CO<sub>2</sub> flux measurements. This estimate does not examine the issue of how atmospheric stability influences the effectiveness of eddy covariance CO<sub>2</sub> measurements. Further field measurements are required to assess whether higher rates of data loss during stable conditions were due to contamination by condensation, or whether the system was incapable of resolving fluxes during these conditions. In the latter case, the potential ocean coverage provided by eddy covariance would be restricted to regions with unstable atmospheric conditions.

#### 4. Conclusion

[43] The results from the Knorr-07 cruises suggest that the air-sea flux of CO<sub>2</sub> was successfully measured by eddy covariance with the system and signal processing techniques described. Significant improvement in the flux measurement was obtained by reducing the Webb correction associated with latent heat flux. The impact of ship motion was reduced by the use of a converted open-path sensor, and an empirical regression technique. The CO<sub>2</sub> sensor used in this study appears to have sufficient sensitivity to resolve the CO<sub>2</sub> flux, even though the ambient fluctuations lie below the RMS noise level of the sensor. This is due to the strong noise filter imposed by the covariance of atmospheric CO<sub>2</sub> with vertical wind. A significant increase in the signal-to-noise characteristics of the CO<sub>2</sub> sensor (i.e., by a factor of 10) would be needed to directly obtain reliable statistics and spectra of atmospheric CO<sub>2</sub> fluctuations.

[44] In the past, large uncertainties associated with the Webb and motion corrections have limited the use of eddy covariance to regions of large air-sea CO<sub>2</sub> fluxes. To date, eddy covariance studies of air-sea CO<sub>2</sub> flux have been conducted only in a few “hotspots” such as the North Atlantic during boreal spring [*McGillis et al.*, 2001] and the southern equatorial Pacific during boreal winter [*McGillis et al.*, 2004], where the air-sea pCO<sub>2</sub> differences are large. To fully constrain the air-sea CO<sub>2</sub> flux, and to explore the factors controlling air-sea gas exchange, it is important to obtain much broader geographic and temporal coverage of the oceans. The results of this study suggest that air-sea CO<sub>2</sub> flux measurements should be possible over much of the world’s oceans. This increase in potential ocean coverage will expand the range of environmental conditions under which the process of air-sea CO<sub>2</sub> exchange can be studied, and raises the possibility of using eddy covariance for validation of air-sea CO<sub>2</sub> flux climatologies.

[45] **Acknowledgments.** Thanks go to Liz Caporelli, Captains Kent Sheasley and George Silva, the WHOI support staff and R/V *Knorr* crew, Cyril McCormick, Jim Albrecht, Warren DeBruyn, George Burba, Bob Eckles, and the Ministry for Foreign Affairs of Iceland. This work was supported by NSF Atmospheric Chemistry (ATM0426314) and is a contribution to U.S. SOLAS. MODIS chlorophyll data are from Ocean-Color web site (<http://oceancolor.gsfc.nasa.gov>).

#### References

Blomquist, B. W., C. W. Fairall, B. J. Huebert, D. J. Kieber, and G. R. Westby (2006), DMS sea-air transfer velocity: Direct measurements by

- eddy covariance and parameterization based on the NOAA/COARE gas transfer model, *Geophys. Res. Lett.*, *33*, L07601, doi:10.1029/2006GL025735.
- Broecker, W. S., J. R. Ledwell, T. Takahashi, R. Weiss, L. Merlivat, L. Memery, B. Jahne, and K. Otto Munnich (1986), Isotopic versus micrometeorologic ocean CO<sub>2</sub> fluxes: A serious conflict, *J. Geophys. Res.*, *91*(C9), 10,517–10,527, doi:10.1029/JC091iC09p10517.
- Edson, J. B., A. A. Hinton, K. E. Prada, J. E. Hare, and C. W. Fairall (1998), Direct covariance flux estimates from mobile platforms at sea, *J. Atmos. Oceanic Technol.*, *15*(2), 547–562, doi:10.1175/1520-0426(1998)015<0547:DCFEM>2.0.CO;2.
- Foken, T., and B. Wichura (1996), Tools for quality assessment of surface-based flux measurements, *Agric. For. Meteorol.*, *78*(1–2), 83–105, doi:10.1016/0168-1923(95)02248-1.
- Hristov, T. S., S. D. Miller, and C. A. Friehe (2003), Dynamical coupling of wind and ocean waves through wave-induced air flow, *Nature*, *422*(6927), 55–58.
- Ibrom, A., E. Dellwik, H. Flyvbjerg, N. O. Jensen, and K. Pilegaard (2007), Strong low-pass filtering effects on water vapour flux measurements with closed-path eddy correlation systems, *Agric. For. Meteorol.*, *147*(3–4), 140–156, doi:10.1016/j.agrformet.2007.07.007.
- Iwata, T., K. Yoshikawa, Y. Higuchi, T. Yamashita, S. Kato, and E. Ohtaki (2005), The spectral density technique for the determination of CO<sub>2</sub> flux over the ocean, *Boundary Layer Meteorol.*, *117*(3), 511–523, doi:10.1007/s10546-005-2773-4.
- Jacobs, C., W. Kohsiek, and W. Oost (1999), Air-sea fluxes and transfer velocity of CO<sub>2</sub> over the North Sea: Results from ASGAMAGE, *Tellus, Ser. B*, *51*(3), 629–641, doi:10.1034/j.1600-0889.1999.t01-2-00005.x.
- Kaimal, J. C., and J. J. Finnigan (1994), *Atmospheric Boundary Layer Flows*, Oxford Univ. Press, New York.
- Kaimal, J. C., J. C. Wyngaard, Y. Izumi, and O. R. Cote (1972), Spectral characteristics of surface-layer turbulence, *Q. J. R. Meteorol. Soc.*, *98*(417), 563–589, doi:10.1002/qj.49709841707.
- Kondo, F., and O. Tsukamoto (2007), Air-sea CO<sub>2</sub> flux by eddy covariance technique in the equatorial Indian Ocean, *J. Oceanogr.*, *63*(3), 449–456, doi:10.1007/s10872-007-0040-7.
- Lenschow, D. H., and M. R. Raupach (1991), The attenuation of fluctuations in scalar concentrations through sampling tubes, *J. Geophys. Res.*, *96*, 15,259–15,268, doi:10.1029/91JD01437.
- Leuning, R., and M. J. Judd (1996), The relative merits of open-and closed-path analysers for measurement of eddy fluxes, *Global Change Biol.*, *2*(3), 241–253, doi:10.1111/j.1365-2486.1996.tb00076.x.
- Leuning, R., and J. Moncrieff (1990), Eddy-covariance CO<sub>2</sub> flux measurements using open-and closed-path CO<sub>2</sub> analysers: Corrections for analyser water vapour sensitivity and damping of fluctuations in air sampling tubes, *Boundary Layer Meteorol.*, *53*(1–2), 63–76, doi:10.1007/BF00122463.
- Liss, P. S., and L. Merlivat (1986), Air-sea gas exchange rates: Introduction and synthesis, in *The Role of Air-Sea Exchange in Geochemical Cycling*, edited by P. Buat-Menard, pp. 113–127, Reidel, Dordrecht, Netherlands.
- Marandino, C. A., W. J. De Bruyn, S. D. Miller, and E. S. Saltzman (2007), Eddy correlation measurements of the air/sea flux of dimethylsulfide over the North Pacific Ocean, *J. Geophys. Res.*, *112*, D03301, doi:10.1029/2006JD007293.
- Massman, W. J. (2000), A simple method for estimating frequency response corrections for eddy covariance systems, *Agric. For. Meteorol.*, *104*(3), 185–198, doi:10.1016/S0168-1923(00)00164-7.
- McGillis, W. R., J. B. Edson, J. E. Hare, and C. W. Fairall (2001), Direct covariance air-sea CO<sub>2</sub> fluxes, *J. Geophys. Res.*, *106*(C8), 16,729–16,746, doi:10.1029/2000JC000506.
- McGillis, W. R., et al. (2004), Air-sea CO<sub>2</sub> exchange in the equatorial Pacific, *J. Geophys. Res.*, *109*, C08S02, doi:10.1029/2003JC002256.
- Miller, S. D., M. L. Goulden, M. C. Menton, H. R. da Rocha, and H. C. de Freitas (2004), Biometric and micrometeorological measurements of tropical forest carbon balance, *Ecol. Appl.*, *14*(SP4), doi:10.1890/02-6005.
- Miller, S. D., T. S. Hristov, J. B. Edson, and C. A. Friehe (2008), Platform motion effects on measurements of turbulence and air-sea exchange over the open ocean, *J. Atmos. Oceanic Technol.*, *25*, 1683–1694, doi:10.1175/2008JTECHO547.1.
- Miller, S. D., C. A. Marandino, W. J. DeBruyn, and E. S. Saltzman (2009), Eddy correlation carbon dioxide and dimethylsulfide air-sea gas exchange in the North Atlantic, *Geophys. Res. Lett.*, *36*, L15816, doi:10.1029/2009GL038907.
- Moore, C. J. (1986), Frequency response corrections for eddy correlation systems, *Boundary Layer Meteorol.*, *37*(1–2), 17–35, doi:10.1007/BF00122754.
- Nightingale, P. D., G. Malin, C. S. Law, A. J. Watson, P. S. Liss, M. I. Liddicoat, J. Boutin, and R. C. Upstill-Goddard (2000), In situ evaluation of air-sea gas exchange parameterizations using novel conservative and volatile tracers, *Global Biogeochem. Cycles*, *14*(1), 373–387, doi:10.1029/1999GB900091.
- Pedrerros, R., G. Dardier, H. Dupuis, H. C. Graber, W. M. Drennan, A. Weill, C. Guérin, and P. Nacass (2003), Momentum and heat fluxes via the eddy correlation method on the R/V *L'Atalante* and an ASIS buoy, *J. Geophys. Res.*, *108*(C11), 3339, doi:10.1029/2002JC001449.
- Saha, S., S. Nadiga, C. Thiaw, J. Wang, W. Wang, Q. Zhang, H. M. VandenDool, H. L. Pan, S. Moorthi, and D. Behringer (2006), The NCEP climate forecast system, *J. Clim.*, *19*(15), 3483–3517, doi:10.1175/JCLI3812.1.
- Smith, S. D., and E. P. Jones (1985), Evidence for wind-pumping of air-sea exchange based on direct measurements of CO<sub>2</sub> fluxes, *J. Geophys. Res.*, *90*(C1), 869–875, doi:10.1029/JC090iC01p00869.
- Smith, S. D., and E. P. Jones (1986), Isotopic and micrometeorological ocean CO<sub>2</sub> fluxes: Different time and space scales, *J. Geophys. Res.*, *91*(C9), 10,529–10,532, doi:10.1029/JC091iC09p10529.
- Stull, R. B. (1988), *An Introduction to Boundary Layer Meteorology*, Kluwer Acad., Dordrecht, Netherlands.
- Takahashi, T., R. A. Feely, R. F. Weiss, R. H. Wanninkhof, D. W. Chipman, S. C. Sutherland, and T. T. Takahashi (1997), Global air-sea flux of CO<sub>2</sub>: An estimate based on measurements of sea-air pCO<sub>2</sub> difference, *Proc. Natl. Acad. Sci. U. S. A.*, *94*(16), 8292–8299.
- Wanninkhof, R. (1992), Relationship between wind speed and gas exchange over the ocean, *J. Geophys. Res.*, *97*(C5), 7373–7382, doi:10.1029/92JC00188.
- Webb, E. K., G. I. Pearman, and R. Leuning (1980), Correction of flux measurements for density effects due to heat and water vapour transfer, *Q. J. R. Meteorol. Soc.*, *106*(447), 85–100, doi:10.1002/qj.49710644707.
- Yelland, M. J., B. I. Moat, R. W. Pascal, and D. I. Berry (2002), CFD model estimates of the airflow distortion over research ships and the impact on momentum flux measurements, *J. Atmos. Oceanic Technol.*, *19*(10), 1477–1499, doi:10.1175/1520-0426(2002)019<1477:CMEOTA>2.0.CO;2.

C. Marandino, Leibniz Institut für Meereswissenschaften (IFM-GEO-MAR), D-24105 Kiel, Germany.

S. D. Miller, Atmospheric Sciences Research Center, State University of New York at Albany, 251 Fuller Rd. L317, Albany, NY 12203, USA. (smiller@albany.edu)

E. S. Saltzman, Earth System Science, University of California, Irvine, CA 92697-3100, USA.